increase OPN mRNA and decrease iNOS mRNA in cardiac myocytes and microvascular endothelium (CMEC), suggesting that the suppression of iNOS by glucocorticoids in CMEC could be partially mediated by OPN [24].

These findings suggest that endogenous OPN may function as a counter-regulator of iNOS in a variety of pathological conditions. We previously reported that OPN and iNOS mRNA were coinduced in a murine macrophage cell line, RAW 264.7 cells, by treating the cells with LPS and IFN-γ [17]. In addition, OPN mRNA expression was markedly upregulated by NO generated from NO-releasing agents in RAW 264.7 cells [17]. We therefore hypothesized that OPN, which can reduce NO production of macrophages by inhibiting iNOS expression, is induced and expressed on alveolar macrophages in the lungs of ARDS, in which NO plays an important role.

In the present study, we examined OPN expression in the lungs of ARDS patients. In addition, we also produced a murine model for ARDS with LPS treatment and investigated the expression of OPN and iNOS in the lungs. We revealed that endogenous OPN is induced and strongly expressed by alveolar macrophages in the lungs of ARDS patients and murine experimental ARDS model.

Materials and Methods

Patients Characteristics and Tissue Preparation

Paraffin-embedded tissue sections were obtained from the postmortem lung samples of 10 patients (6 men, 4 women) with ARDS who were autopsied at Juntendo University Hospital. ARDS was confirmed according to the American European Consensus Conference definitions, which include acute onset of bilateral infiltrates on chest radiograph, an arterial pO_2-to-inspired O_2 ratio of ≤ 200, and no clinical evidence of elevated left arterial pressure [2]. The patients ranged in age from 36 to 85 years (mean ± S.D. 69.6 ± 15.0). Underlying diseases included sepsis, pneumonia, lung abscess, pulmonary embolism, acute pancreatitis, renal disease, cerebral hemorrhage, hematological disease, and malignant tumor. All patients had been treated with oxygen prior to death, and 4 had been ventilated mechanically. Normal lung tissue samples were obtained from 5 controls who had normal lung tissue surgically removed distal to the lung tumor. Tissue samples were formalin fixed, embedded in paraffin, and cut into 3 μm sections. Informed consent was obtained from either the patient or a responsible relative.

Animals

Specific pathogen-free male ICR mice aged 8 weeks were purchased from Charles River Laboratories, Japan (Tokyo, Japan). The mice were housed in filter-topped cages in an isolation room in the animal care facility with free access to rodent chow and water. All animal experiments were performed according to the Guidelines on Animal Experimentation as established by Juntendo University School of Medicine.

Intratracheal Inoculation of Echericha coli Lipopolysaccharide

Mice were anesthetized with pentobarbitral (50 mg/kg intraperitoneally). The trachea was exposed by midline incision into which a 24-gauge Saflow catheter® (Terumo, Tokyo, Japan) was introduced.

Then the mice were intratrachealy (i.t.) injected 10 μg of *E. coli* LPS (055: B5; Sigma, St. Louis, MI) or 0.05 ml phosphate-buffered saline (PBS). This was followed by 0.5 ml of air on days 0 and 4 on the basis of previous reports that single high-dose LPS injection failed to cause pulmonary edema in animal models, and that additional activation of macrophages, called "priming", was required to induce severe lung injury [7, 25]. The mice were sacrificed for RNA extraction from lungs 12 and 36 h after the second i.t. injection. Mortality rate for i.t. injection was less than 5%.

Bronchoalveolar Lavage (BAL)

Thirty-six hours after the second i.t. injection, bronchoalveolar lavage was performed. The animals were anesthetized before undergoing aortic transection. The sterile polypropylene catheter was secured in the trachea with suture material. The lungs were isolated and lavaged via the trachea with PBS. A total of 2 ml of lavage buffer was used per mouse in 0.5-ml increments. Total cell counts were assessed with a standard hemocytometer. Cellular populations were identified on air-dried cytocentrifuged smears (900 rpm × 2 min) after staining with Diff Quick stain (Wako, Tokyo, Japan). Similarly, treated slides were used for immunocytochemical analyses.

Immunostaining

The expression of OPN in the lungs of ARDS patients and the experimental murine model was assessed by immunohistochemical staining using mouse anti-human OPN monoclonal antibody (10A16; Immuno-Biological Laboratories Co.; Ltd.; Gunma, Japan) and polyclonal rabbit anti-human OPN antibody (IBL) which cross-reacts with mouse OPN, respectively. Immunohistochemical analyses were performed as previously described [16, 20]. Briefly, sections were autoclaved for 15 min at 120°C in 10 mM citrate buffer, pH 6.0 to retrieve the antigen. The sections were then incubated with mouse anti-human OPN antibody and rabbit anti-human OPN antibody diluted 1: 100 for 1 hr at room temperature (RT), respectively. Specific binding was detected through avidin-biotin peroxidase complex formation with a biotin-conjugated second antibody (Vectastain ABC Kit; Vector; Burlingame, CA) and diaminobendizine (Sigma; St. Louis, MI) as substrate. Staining was absent when isotype-matched immunoglobulin was used as the control.

The expression of iNOS in the lungs of ARDS mice was also assessed by immunohistochemical staining using polyclonal rabbit anti-mouse iNOS antibody (Affinity Bioreagents) according to the manufacturer's instructions. Alveolar macrophages were identified by immunoreactivity for anti-human CD68 antibody (Dako; Tokyo, Japan) and BM 8 antibody (BMA; Rheistrasse, Switzerland) which reacts specifically to human and murine macrophages, respectively. Immunohistochemical staining was conducted according to the manufacturer's instructions, whereby, BAL cells were fixed with cold acetone and subjected to the same method as that for immunohistochemistry. Each specimen was examined independently by three observers. In order to prevent observer's bias, samples were coded and examined in a blind manner.

Northern Blot

iNOS cDNA probe was purchased from Cayman Chemical (Ann Arbor, MI). OPN cDNA was amplified from RAW 264.7 cells. Sense primer (5′-GCCTGGATCCTCCCGGTGAAAGTGACT-GAT-3′) contains the *Bam*HI restriction site and the cDNA sequence coding the first seven amino acids of mature OPN. Anti-sense primer AS1 (5′-GTTAGAATTCCTGCTTAATCCTCACTAACA-3′) contains the *Eco*RI restriction site and the cDNA sequence of the six amino acids starting from 19 amino acids C-terminal from the stop codon. Nuclear sequences of the cDNA were verified with a DNA sequencer (Perkin Elmer; Foster City, CA). The PCR product was digested with *Bam*HI and

*Eco*RI, and subcloned into the *Bam*HI and *Eco*RI sites of the pGEX-5X1 vector (Amersham Pharmacia Biotech; Buckinghamshire, England). The template was used as a probe for Northern blots. Total RNAs were extracted from lungs and cells by the guanidium thiocyanate-phenol-chloroform extraction procedure (Tel-test; Friendswood, TX). Total RNAs were electrophoresed in 1% formaldehyde agarose gel and transferred onto a nylon membrane (Amersham Pharmacia Biotech). cDNA probes were labeled with [^{32}P]dCTP (Amersham Pharmacia Biotech) by the random prime method (Takara; Tokyo, Japan).

Prehybridization and hybridization were carried out at 42°C overnight. Filters were washed in 2× SSC, 0.1% SDS twice and in 0.1 × SSC, 0.1% SDS 4 times at 55°C and exposed to the film (Fuji Film; Tokyo, Japan). Filters were also hybridized with a human 28 S ribosomal RNA cDNA probe as a control for loading. Autoradiography bands were quantitated by image analyzer (Fuji Film; Tokyo, Japan).

Measurement of NO Production

NOx, nitrite and nitrate, were determined with an NOx assay kit (Boehringer Mannheim; Mannheim, Germany) according to the manufacturer's instruction [7]. Briefly, 50 µl of BAL fluid, sera, and culture supernatants were reacted with 1 U/ml nitrate reductase and 1 mg/ml NADPH, followed by incubation with an equal volume of Griess reagent (1% sulfanilamide, 0.1% N-1-naphthylethylenediamine dihydrochloride, and 2.5% phosphoric acid) at room temperature for 5 min. Absorbance at 560 nm was determined with a microplate reader (Bio-Rad; Hercules, CA). NOx concentrations were calculated from a standard sodium nitrite curve. All samples were analyzed in triplicate.

Myeloperoxidase Assay

Myeloperoxidase (MPO) was analyzed as described previously [26, 27, 28]. Briefly, 0.12 ml BAL fluid was mixed with 0.88 ml substrate solution (0.1 M citric acid-sodium citrate buffer, pH 5.0, 0.1% o-tolidine in ethanol, 1.5 mM H_2O_2), and absorbance at 440 nm was measured.

Statistics

Statistical analyses were performed by analysis of variance (ANOVA). All data are presented as mean ± S.D. Differences between means were considered statistically significant at $p < 0.05$.

Results

OPN Expression in Lungs of Patients with ARDS

OPN expression was investigated in lung tissues from 10 patients with ARDS. Pathological findings of these patients revealed diffuse alveolar damage, with neutrophils, macrophages, hyaline membranes, protein-rich edema fluid in the alveolar spaces, and disruption of the alveolar epithelium (data not shown). These findings suggested ARDS. Tissue sections were stained with anti-human OPN mAb (clone 10A16) or isotype-matched IgG. As shown in Figure 1A, OPN was strongly expressed by accumulating macrophages in alveolar spaces. Interestingly,

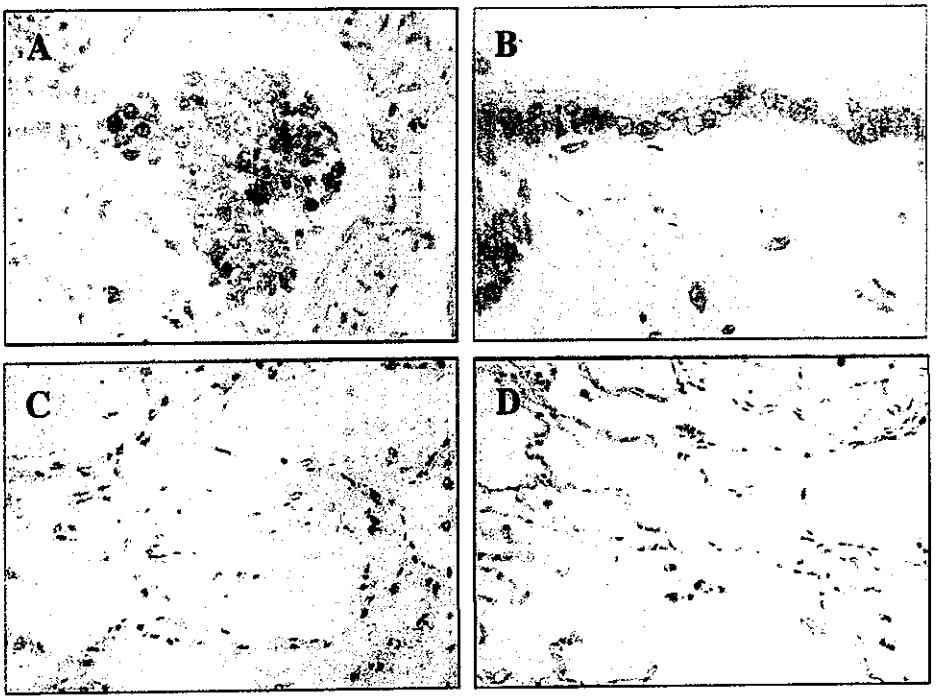

Fig. 1. Immunohistochemical staining of OPN in the lungs of ARDS patients and controls. The lung tissues obtained from ARDS patients (A, B, C) and controls (D) were stained with antibody against OPN. (A) OPN was strongly expressed on macrophages in alveolar spaces in the lungs of ARDS patients. Alveolar epithelial cells were weakly stained for OPN. No staining was observed in (B) bronchial epithelial cells, (C) vascular endothelial and smooth muscle cells in the lungs of ARDS patients, and (D) alveolar macrophages in the lungs of controls. Hematoxylin was used as the counter stain (original magnification: ×100).

OPN-expressing macrophages were aggregated. Interstitial macrophages were weakly stained for OPN.

In contrast, no significant staining was observed on lymphocytes and neutrophils. To verify that OPN-producing cells were indeed macrophages, immunostaining using an antibody against human macrophage antigen CD68 was conducted. OPN-expressing cells were also stained with a mAb specific for CD68, indicating that OPN was expressed predominantly on alveolar macrophages (data not shown). Alveolar epithelial cells were weakly stained for OPN (Fig. 1A). OPN expression on bronchial epithelium, vascular endothelial cells, and smooth muscle cells were not significant (Fig. 1B, C). No staining of these specimens was observed with the isotype control Ab. Normal control lungs did not demonstrate any significant staining for OPN (Fig. 1D). Cellular expression and localization of OPN are summarized in Table 1. These results indicated that OPN was induced and expressed predominantly on alveolar macrophages in the lungs of patients with ARDS.

Table 1. Cellular expression and localization of OPN in the lungs of ARDS patients and normal controls

	ARDS patients (n = 10)	Normal controls (n = 5)
Alveolar macrophages	+ + +	−
Interstitial macrophages	+	−
Lymphocytes	−	−
Neutrophils	−	−
Bronchial epithelial cells	−	−
Alveolar epithelial cells	+	−
Vascular endothelial cells	−	−
Vascular smooth muscle cells	−	−

Staining intensities were scored according to the following scale: −, no staining; +, weak staining; + +, positive staining, + + +, strong staining

Experimental ARDS in Mice

We produced a murine model for ARDS by sequential exposure to LPS. Confirmation of ARDS was conducted with both histological and biochemical analyses. Histological examination of the lungs at 36 h after LPS treatment revealed alveolar wall thickening, edema, parenchymal damage, and accumulation of neutrophils and macrophages in the interstitium, all of which are consistent with ARDS (data not shown). In contrast, PBS-treated mice demonstrated normal lung findings. Wet lung weights were significantly higher in LPS-treated than in PBS-treated mice (Table 2). We next performed bronchoalveolar lavage (BAL). LPS treatment resulted in an increased number of neutrophils and macrophages compared to PBS treatment (Table 2). Protein levels and MPO activity in BAL fluid of LPS-treated mice were also increased (Table 2). We also measured NO_2^-/NO_3^- (NOx) levels in BAL fluid and sera in these mice. Levels of NOx in both BALF and sera of LPS-treated mice were significantly higher than those of the control mice.

Immunostaining of OPN and iNOS Proteins in ARDS Mice Lungs and Bronchoalveolar Lavage Cells

Immunohistochemical analyses were carried out on the lungs obtained at 36 h after the second i.t. injection. OPN and iNOS proteins were absent in the lungs of PBS-treated mice (data not shown). In contrast, alveolar macrophages in the lungs of LPS-treated mice were positive for OPN and iNOS immunoreactivity (data not shown). To further identify cells positive for OPN and iNOS proteins in the lungs of LPS- or PBS-treated mice, immunocytochemical analyses were also performed on BAL cells (Fig. 2). We first ascertained that aggregated cells were identified as alveolar macrophages by positive immunoreactivity to BM 8 antibody (data not shown). As expected, both iNOS and OPN proteins were strongly positive predominantly in the alveolar macrophages (Fig. 2A, B). Neither iNOS nor OPN

Table 2. Comparison of wet lung weight, number of neutrophils and macrophages, and biochemical parameters of acute lung injury between in LPS- and PBS-treated mice

	Wet lung weight[a] (mg)	Neutrophils in BAL[b] ($\times 10^3$/ml)	Macrophages in BAL[b] ($\times 10^4$/ml)	Protein in BAL fluid[c] (mg/ml)	MPO activity in BALF[d] (ΔOD440/min)	NOx in BALF[e] (μM)	NOx in serum[e] (μM)
LPS	162 ± 28**	1250 ± 54***	30 ± 16**	1.46 ± 0.6**	0.017 ± 0.01**	4.8 ± 1.5**	63 ± 57*
PBS	65 ± 12	4.8 ± 8.2	6.5 ± 0.9	0.065 ± 0.01	0.0005 ± 0.0005	2.2 ± 0.5	33 ± 32

[a] $n = 4$ for LPS i.t., $n = 4$ for PBS i.t.
[b] $n = 6$ for LPS i.t., $n = 5$ for PBS i.t.
[c] $n = 6$ for LPS i.t., $n = 8$ for PBS i.t.
[d] $n = 6$ for LPS i.t., $n = 7$ for PBS i.t.
[e] $n = 6$ for LPS i.t., $n = 7$ for PBS i.t.*$p < 0.05$ vs. PBS i.t. **$p < 0.01$ vs. PBS i.t. ***$p < 0.001$ vs. PBS i.t.

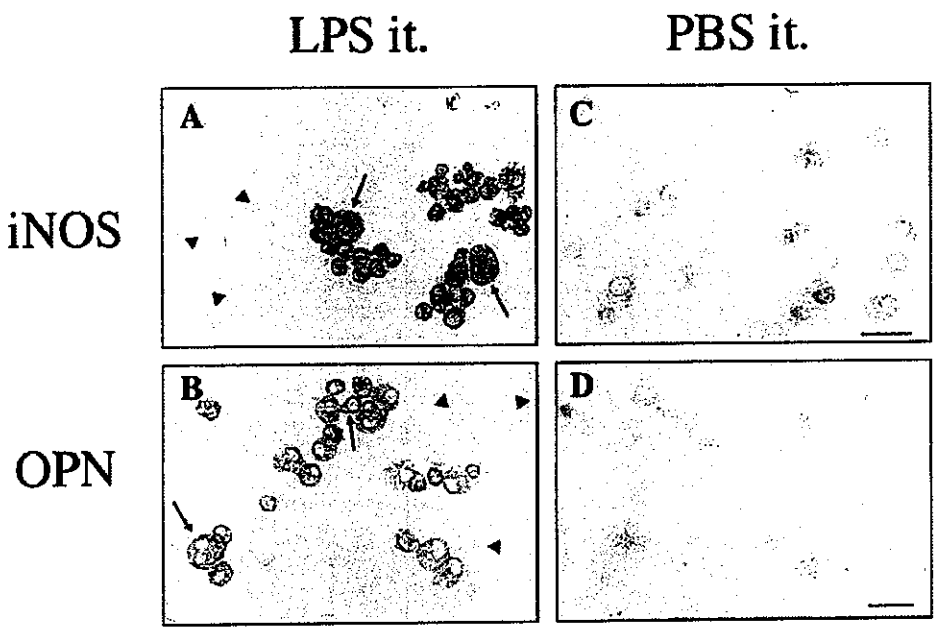

Fig. 2. Immunocytochemical staining of BAL cells from LPS- and PBS-treated mice for iNOS (A, C) and OPN (B, D) protein. BAL cells recovered from mice at 36 h after the second i.t. injection with LPS or PBS which were stained with a polyclonal antibody against iNOS (A: LPS, C: PBS) or OPN (B: LPS, D: PBS). Arrows indicate macrophages showing positive staining for iNOS and positive staining for OPN. Arrowheads indicate neutrophils showing negative staining for iNOS and for OPN. Bar indicates 10 μm in Figures 2C and 2D.

were prominent in neutrophils (Fig. 2A, B) or all BAL cells obtained from PBS-treated mice (Fig. 2C, D) These data indicate that OPN and iNOS proteins were coinduced predominantly in alveolar macrophages in the lungs of ARDS mice.

Expression of OPN and iNOS mRNA in Lungs of ARDS Mice

We also investigated the expression of OPN and iNOS mRNA in the whole lungs after LPS treatment *in vivo* (Fig. 3A, B). iNOS mRNA reached its maximum at 12 h after treatment and then decreased rapidly at 36 h. In contrast, OPN mRNA began to increase at 12 h with a lag time and was prominent at 36 h. Thus, iNOS and OPN mRNAs were coinduced by LPS in the lungs, but OPN mRNA was induced more slowly than iNOS mRNA. In contrast, neither mRNAs were induced in the lungs after PBS treatment (data not shown).

Discussion

In the current study, we revealed that OPN is strongly expressed by alveolar macrophages in the lungs of ARDS patients. In addition, we produced a murine

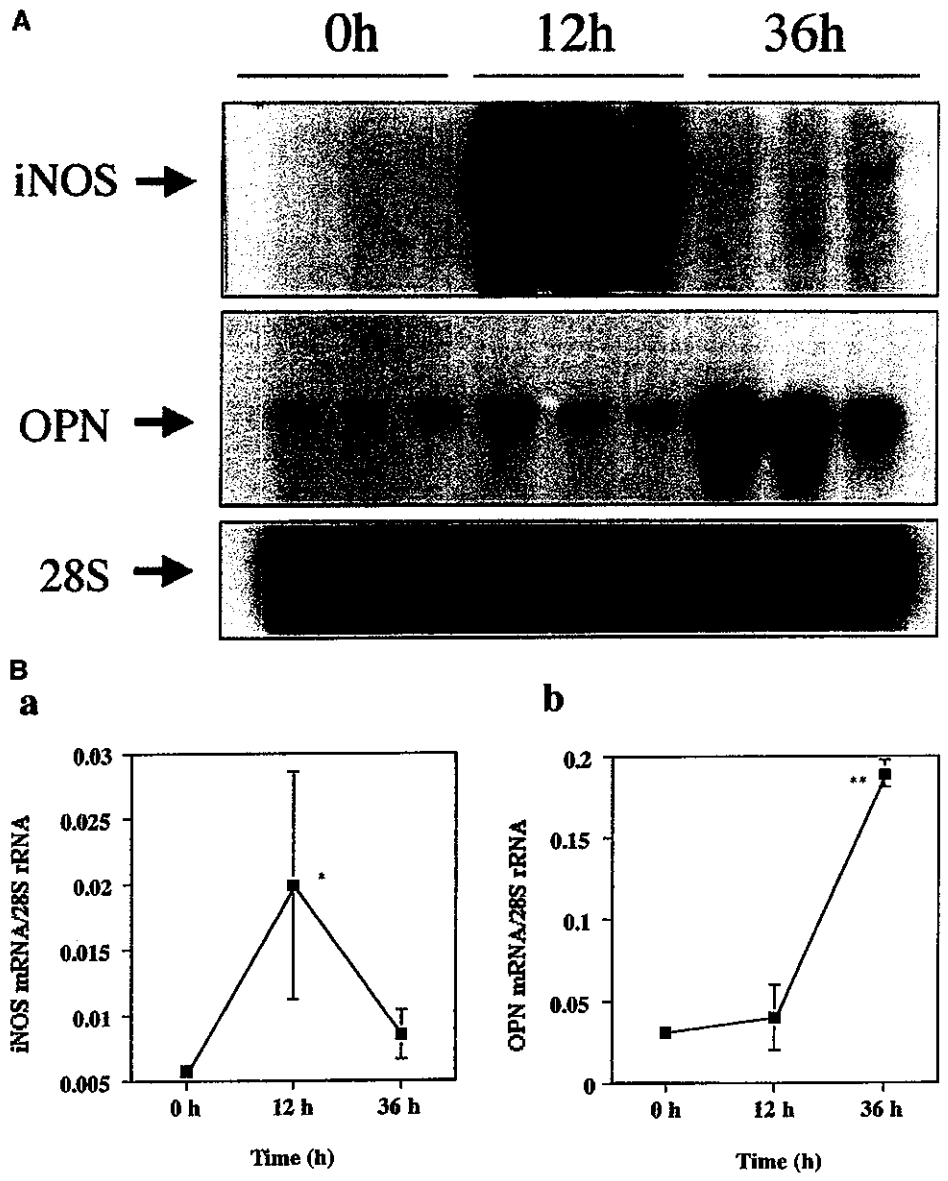

Fig. 3. Induction of iNOS and OPN mRNA in the lungs of LPS-treated mice with Northern blot. (A) Total RNAs were isolated from lungs of 3 mice at the indicated time period (h) after treatment with LPS (10 μg/50 μl) or PBS (50 μl). RNAs (10 μg) were subjected to blot analysis. Upper panels indicate the expression of iNOS or OPN mRNA. Lower panel shows 28S rRNA as the control. (B) The signals were quantified using a computerized image analyzer. Calculated ratios iNOS/28S signal (a) and OPN/28S signal (b) are shown in Figure 3B. Data are presented as the mean ± SD of three independent experiments. $^{*}p < 0.05$ vs. time 0, $^{**}p < 0.001$ vs. time 0.

model for ARDS with LPS treatment and investigated the expression of OPN and iNOS in the lungs. OPN protein was significantly induced by alveolar macrophages and OPN mRNA was induced more slowly than iNOS mRNA. These results, together with previous findings, suggest that OPN, which can reduce NO production of macrophages by inhibiting iNOS expression, is significantly induced and strongly expressed on alveolar macrophages in the lungs of ARDS. Although we were unable to demonstrate direct evidence that OPN is implicated in the pathogenesis of ARDS, it is possible that it has beneficial effects in protecting lung tissues from damage by reactive nitrogen intermediates by inhibiting iNOS expression in macrophage.

What actually induces and upregulates OPN expression in the lungs of ARDS is unclear. Previous reports have indicated that tumor necrosis factor-α (TNF-α) plays a key role in the pathogenesis of ARDS [1]. The expression of OPN mRNA was revealed to be increased in the macrophage cell line in the presence of TNF-α, as well as in alveolar macrophages in transgenic mice that were engineered to express TNF-α in type II pneumocytes [29]. Other than TNF-α, various mediators, including IL-1β, PDGF, and TGF-β, have also been demonstrated to upregulate OPN transcription and stimulate OPN expression [30]. It has been demonstrated that iNOS is strongly expressed on alveolar macrophages of human lungs predominantly during the early stage of ARDS following sepsis [31]. In addition, increased levels of NO production were demonstrated in the lungs of ARDS patients [32]. We have previously reported that increased amounts of NO generated by NO-releasing agents directly upregulates OPN expression in the murine macrophage cell line [17]. Therefore, induction of OPN appears to be mediated by NO and/or various inflammatory mediators induced in the lungs of ARDS.

Kinetic studies in a murine experimental model revealed that OPN mRNA is induced much more slowly and with a time lag in the lungs of LPS-treated mice, whereas iNOS mRNA is induced more rapidly. Immunohistochemical studies suggested that OPN mRNA were mainly derived from macrophages. We previously reported that iNOS and OPN are coinduced in the murine macrophage cell line stimulated with LPS and IFN-γ, and induction of OPN mRNA was also slower than that of iNOS mRNA *in vitro* [17]. Thus, the profile of kinetics for iNOS and OPN mRNA induction *in vivo* resembled that of an *in vitro* murine macrophage cell line on treatment of cells with LPS and IFN-γ. We also previously demonstrated that OPN mRNA induction was markedly suppressed by inhibiting iNOS mRNA by addition of the specific iNOS inhibitor S-2-aminoethyl isothiourea dihydrobromide. Moreover, OPN mRNA expression was significantly upregulated by NO generated by NO-releasing agent spermine NONOate. Guo et al. also demonstrated that OPN gene transcription and promotor activity is upregulated by NO in endotoxin- and cytokine- stimulated macrophages [33]. These findings suggested that NO generated by iNOS upregulates OPN expression in macrophages stimulated with LPS. Together with these previous findings, it is possible that delayed induction of OPN is caused by excessive production of NO by macrophages in ARDS.

Conclusively, our study revealed that OPN is significantly induced and strongly expressed on alveolar macrophages in the lungs of ARDS patients and a

murine experimental model. Our data suggest that induced OPN may have beneficial effects, protecting tissue from damage by toxic reactive nitrogen intermediates, by inhibiting iNOS expression in macrophages. However, further studies are necessary.

Acknowledgments. We thank Dr. Y. Ishii for her excellent advise. This work was supported in part by Grant-in-Aid for Scientific Research 13670616 (K.T.) and 14770279 (F.T.) from the Ministry of Education, Culture, Sports, Science, and Technology of Japan.

References

1. Ware LB, Matthay MA (2000) The acute respiratory distress syndrome. N Engl J Med 342:1334–1349
2. Bernard GR, Artigas A, Brigham KL, et al. (1994) The American-European Consensus Conference on ARDS. Definitions, mechanisms, relevant outcomes, and clinical trial coordination. Am J Respir Crit Care Med 149:818–824
3. Hogg JC (1987) Neutrophil kinetics and lung injury. Physiol Rev 67:1249–1295
4. Lee CT, Fein AM, Lippmann M, Holtzman H, Kimbel P, Weinbaum G (1981) Elastolytic activity in pulmonary lavage fluid from patients with adult respiratory-distress syndrome. N Engl J Med 304:192–196
5. Thommasen HV, Russell JA, Boyko WJ, Hogg JC (1984) Transient leucopenia associated with adult respiratory distress syndrome. Lancet 1:809–812
6. Tasaka S, Ishizaka A, Urano T, et al. (1995) BCG priming enhances endotoxin-induced acute lung injury independent of neutrophils. Am J Respir Crit Care Med 152:1041–1049
7. Shellito JE, Kolls JK, Summer WR (1995) Regulation of nitric oxide release by macrophages after intratracheal lipopolysaccharide. Am J Respir Cell Mol Biol 13:45–53
8. Wizemann TM, Gardner CR, Laskin JD, et al. (1994) Production of nitric oxide and peroxynitrite in the lung during acute endotoxemia. J Leukoc Biol 56:759–768
9. Beckman JS, Beckman TW, Chen J, Marshall PA, Freeman BA (1990) Apparent hydroxyl radical production by peroxynitrite: implications for endothelial injury from nitric oxide and superoxide. Proc Natl Acad Sci USA 87:1620–1624
10. Arkovitz MS, Wispe JR, Garcia VF, Szabo C (1996) Selective inhibition of the inducible isoform of nitric oxide synthase prevents pulmonary transvascular flux during acute endotoxemia. J Pediatr Surg 31:1009–1015
11. Wu CC, Chen SJ, Szabo C, Thiemermann C, Vane JR (1995) Aminoguanidine attenuates the delayed circulatory failure and improves survival in rodent models of endotoxic shock. Br J Pharmacol 114:1666–1672
12. Kristof AS, Goldberg P, Laubach V, Hussain SN (1998) Role of inducible nitric oxide synthase in endotoxin-induced acute lung injury. Am J Respir Crit Care Med 158:1883–1889
13. Denhardt DT, Guo X (1993) Osteopontin: a protein with diverse functions. Faseb J 7:1475–1482
14. Takahashi K, Takahashi F, Tanabe KK, Takahashi H, Fukuchi Y (1998) The carboxyl-terminal fragment of osteopontin suppresses arginine-glycine-asparatic acid-dependent cell adhesion. Biochem Mol Biol Int 46:1081–1092
15. Denhardt DT, Noda M, O'Regan AW, Pavlin D, Berman JS (2001) Osteopontin as a means to cope with environmental insults: regulation of inflammation, tissue remodeling, and cell survival. J Clin Invest 107:1055–1061
16. Zhang J, Takahashi K, Takahashi F, et al. (2001) Differential osteopontin expression in lung cancer. Cancer Lett 171:215–222
17. Takahashi F, Takahashi K, Maeda K, Tominaga S, Fukuchi Y (2000) Osteopontin is induced by nitric oxide in RAW 264.7 cells. IUBMB Life 49:217–221

18. O'Regan AW, Chupp GL, Lowry JA, Goetschkes M, Mulligan N, Berman JS (1999) Osteopontin is associated with T cells in sarcoid granulomas and has T cell adhesive and cytokine-like properties *in vitro*. J Immunol 162:1024–1031
19. Takahashi F, Akutagawa S, Fukumoto H, et al. (2002) Osteopontin induces angiogenesis of murine neuroblastoma cells in mice. Int J Cancer 98:707–712
20. Takahashi F, Takahashi K, Okazaki T, et al. (2001) Role of osteopontin in the pathogenesis of bleomycin-induced pulmonary fibrosis. Am J Respir Cell Mol Biol 24:264–271
21. Rollo EE, Laskin DL, Denhardt DT (1996) Osteopontin inhibits nitric oxide production and cytotoxicity by activated RAW264.7 macrophages. J Leukoc Biol 60:397–404
22. Hwang SM, Lopez CA, Heck DE, et al. (1994) Osteopontin inhibits induction of nitric oxide synthase gene expression by inflammatory mediators in mouse kidney epithelial cells. J Biol Chem 269:711–715
23. Scott JA, Weir ML, Wilson SM, Xuan JW, Chambers AF, McCormack DG (1998) Osteopontin inhibits inducible nitric oxide synthase activity in rat vascular tissue. Am J Physiol 275:H2258–H2265
24. Singh K, Balligand J, Fisher T, Smith TW, Kelly RA (1995) Glucocorticoids increase osteopontin expression in cardiac myocytes and microvascular endothelial cells. J Biol Chem 270:28471–28478
25. Wollert PS, Menconi MJ, Wang H, et al. (1994) Prior exposure to endotoxin exacerbates lipopolysaccharide-induced hypoxemia and alveolitis in anesthetized swine. Shock 2:362–369
26. Szarka RJ, Wang N, Gordon L, Nation PN, Smith RH (1997) A murine model of pulmonary damage induced by lipopolysaccharide via intranasal instillation. J Immunol Methods 202:49–57
27. Baggiolini M, Hirsch JG, De Duve C (1969) Resolution of granules from rabbit heterophil leukocytes into distinct populations by zonal sedimentation. J Cell Biol 40:529–541
28. Avila JL, Convit J (1973) Studies on human polymorphonuclear leukocyte enzymes. I. Assay of acid hydrolases and other enzymes. Biochim Biophys Acta 293:397–408
29. Miyazaki Y, Tashiro T, Higuchi Y, et al. (1995) Expression of osteopontin in a macrophage cell line and in transgenic mice with pulmonary fibrosis resulting from the lung expression of a tumor necrosis factor-alpha transgene. Ann N Y Acad Sci 760:334–341
30. Rodan GA (1995) Osteopontin overview. Ann N Y Acad Sci 760:761–765
31. Kobayashi A, Hashimoto S, Kooguchi K, et al. (1998) Expression of inducible nitric oxide synthase and inflammatory cytokines in alveolar macrophages of ARDS following sepsis. Chest 113:1632–1639
32. Sittipunt C, Steinberg KP, Ruzinski JT, et al. (2001) Nitric oxide and nitrotyrosine in the lungs of patients with acute respiratory distress syndrome. Am J Respir Crit Care Med 163:503–510
33. Guo H, Cai CQ, Schroeder RA, Kuo PC (2001) Osteopontin is a negative feedback regulator of nitric oxide synthesis in murine macrophages. J Immunol 166:1079–1086

Accepted for publication: April 12, 2004

Dissection of the role of MHC class II A and E genes in autoimmune susceptibility in murine lupus models with intragenic recombination

Danqing Zhang*, Keishi Fujio†, Yi Jiang‡, Jingyuan Zhao*, Norihiro Tada§, Katsuko Sudo¶, Hiromichi Tsurui*, Kazuhiro Nakamura*, Kazuhiko Yamamoto†, Hiroyuki Nishimura‖, Toshikazu Shirai*, and Sachiko Hirose*,**

*Second Department of Pathology and §Atopy Research Center, Juntendo University School of Medicine, Tokyo 113-8421, Japan; †Department of Allergy and Rheumatology, Graduate School of Medicine, University of Tokyo, Tokyo 113-0033, Japan; ‡Central Laboratory of First Clinical College, China Medical University, ShenyCang 110001, China; ¶Animal Research Center, Tokyo Medical University, Tokyo 160-8402, Japan; and ‖Toin Human Science and Technology Center, Department of Biomedical Engineering, Toin University of Yokohama, Yokohama 225-8502, Japan

Communicated by N. Avrion Mitchison, University College London, London, United Kingdom, August 8, 2004 (received for review July 7, 2004)

Systemic lupus erythematosus (SLE) is a multigenic autoimmune disease, and the major histocompatibility complex (MHC) class II polymorphism serves as a key genetic element. In SLE-prone (NZB × NZW)F_1 mice, the MHC H-$2^{d/z}$ heterozygosity (H-2^d of NZB and H-2^z of NZW) has a strong impact on disease; thus, congenic H-$2^{d/d}$ homozygous F_1 mice do not develop severe disease. In this study, we used *Ea*-deficient intra-H-2 recombination to establish $A^{d/d}$-congenic (NZB × NZW)F_1 mice, with or without E molecule expression, and dissected the role of class II A and E molecules. Here we found that $A^{d/d}$ homozygous F_1 mice lacking E molecules developed severe SLE similar to that seen in wild-type F1 mice, including lupus nephritis, autoantibody production, and spontaneously occurring T cell activation. Additional evidence revealed that E molecules prevent the disease in a dose-dependent manner; however, the effect is greatly influenced by the haplotype of A molecules, because wild-type H-$2^{d/z}$ F_1 mice develop SLE, despite E molecule expression. Studies on the potential of dendritic cells to present a self-antigen chromatin indicated that dendritic cells from wild-type F_1 mice induced a greater response of chromatin-specific T cells than did those from $A^{d/d}$ F_1 mice, irrespective of the presence or absence of E molecules, suggesting that the self-antigen presentation is mediated by A, but not by E, molecules. Our mouse models are useful for analyzing the molecular mechanisms by which MHC class II regions regulate the process of autoimmune responses.

Systemic lupus erythematosus (SLE) is a systemic autoimmune disease characterized by the appearance of autoantibodies to several nuclear components. The deposition of formed immune complexes mediates the disease in a wide variety of tissues and organs, including the kidney and the vascular system. There is evidence that the development of SLE is under the control of multiple susceptibility genes (1). Among these, genes in the major histocompatibility complex (MHC) have been implicated as a key genetic element. Because SLE is an autoantibody-mediated disease, MHC class II polymorphisms are probably involved in the pathogenesis. However, because of the complex multifactorial inheritance and heterogeneity of SLE, and because of the linkage disequilibrium that exists among the class I, II, and III genes within the MHC complex, the absolute contribution of individual MHC class II loci has been difficult to dissect. Thus, our knowledge of the molecular mechanism of MHC class II contribution to SLE remains incomplete.

Substantial progress in research in this area has been achieved through studies using SLE-prone mice with genetic recombination and manipulation of MHC (H-2) genes. In (NZB × NZW)F_1 mice that spontaneously develop disease closely resembling human SLE, the disease is strongly associated with H-2 haplotypes from both parents (H-2^d from NZB and H-2^z from NZW) (2–6). Genetic dissection by producing H-2-congenic mice revealed that an early onset of severe SLE occurs in only heterozygous H-$2^{d/z}$ mice and not in homozygous H-$2^{d/d}$ and H-$2^{z/z}$ mice (2, 3, 5). Although both A and E class II molecules may be involved, evidence has suggested that mixed haplotype class II A$\alpha^d\beta^z$ molecules are responsible for the pathogenesis by promoting the production of pathogenic high-affinity IgG autoantibodies to nuclear components (7, 8).

In contrast to class II A molecules, E molecules are suggested to be a suppressive genetic element for SLE. This notion was based mainly on the results obtained by using a transgene technique. A BXSB strain of mouse, another spontaneous SLE model, carries H-2^b haplotype and expresses A^b, but not E, molecules, because of a defect in the *Ea* gene (9). The development of BXSB disease is closely associated with the H-2^b haplotype (10) and is almost completely prevented by a transgene encoding Eα^d chains (11). Similar findings were noted in the nonobese diabetic (NOD) mouse, a model of spontaneous autoimmune diabetes. NOD mice express class II A^{g7}, but not E, molecules, because of a defect in the *Ea* gene (12). Evidence indicated that whereas the class II A^{g7} gene is critical for the disease susceptibility (13), the transgenic introduction of Eα^d or Eα^k does prevent the disease (14–16). Thus, A and E molecules seem to provide the susceptible and protective genetic elements for autoimmune diseases, respectively, at least in these mouse models.

Nevertheless, the conclusion awaits further studies, because the transgene possibly induces unexpected improper effects on immune cells. For example, unpaired or mispaired transgene-derived class II molecules can be toxic to B cell maturation (17). Furthermore, there are reports suggesting that excessively generated transgenic Eα^d molecules bind to A molecules, thereby decreasing the availability of A molecules for antigen presentation (18), and that overexpression of E molecules suppresses expression levels of endogenously encoded A molecules (19). In the (NZB × NZW)F_1 model, severe SLE occurs despite the presence of intact E molecules. To examine the role of A and E molecules in (NZB × NZW)F_1 lupus, we generated several kinds of congenic (NZB × NZW)F_1 mice with intra-MHC recombination at the *E* subregion, taking advantage of natural recombinants, including those we found among ≈3,000 meiosis in crosses of NZB strains.

Materials and Methods

Mice. NZB (H-2^d) and NZW (H-2^z) mice were purchased from the Shizuoka Laboratory Animal Center (Shizuoka, Japan) and were maintained in our animal facility. The H-2-congenic

Abbreviations: DC, dendritic cell; NOD, nonobese diabetic; SLE, systemic lupus erythematosus; TCR, T cell receptor.

**To whom correspondence should be addressed at: Second Department of Pathology, Juntendo University School of Medicine, 2-1-1, Hongo, Bunkyo-ku, Tokyo 113-8421, Japan. E-mail: sacchi@med.juntendo.ac.jp.

www.pnas.org/cgi/doi/10.1073/pnas.0405807101

Table 1. H-2 haplotypes of established MHC-congenic and intra-MHC recombinant-congenic New Zealand strains of mice

Strains	H-2 haplotype	*K*	*Ab*	*Aa*	*Eb*		*Ea*		*Tnfa*	*D*
NZB	d	d	d	d	d		d		d	d
NZB.GD	g2	d	d	d	d	//	b		b	b
NZW.GD	g2	d	d	d	d	//	b		b	b
NZB.GDr	g2r	d	d	d	d		d	//	b	b
NZW.H-2^d	d	d	d	d	d		d		d	d
(NZB × NZW.H-2^d)F_1	d/d	d	d	d	d		d		d	d
(NZB × NZW.GD)F_1	d/g2	d	d	d	d		d/b		d/b	d/b
(NZB.GDr × NZW.GD)F_1	g2r/g2	d	d	d	d		d/b		b	b
(NZB.GD × NZW.GD)F_1	g2/g2	d	d	d	d	//	b		b	b

//, Intra-H-2 recombination site between d and b haplotype.

NZW.H-2^d (2, 3, 5) strain was established by selective backcrossing of (NZB × NZW)F_1 to NZW for 15 generations. NZB.GD (H-2^{g2}) (20) and NZW.GD strains were established by selective backcrossing of (B10.GD × NZB)F_1 and (B10.GD × NZW)F_1 with NZB and with NZW mice, respectively, for 15 generations. The NZB strain with an intragenic recombination between *Ea* of NZB and *Tnfa* of NZB.GD was obtained in crosses of NZB and NZB.GD strains and was tentatively designated NZB.GDr. Alleles at the H-2 loci in established H-2-congenic and recombinant H-2-congenic New Zealand mice are shown in Table 1. These mice were crossed to produce (NZB × NZW)F_1 hybrids with the same d haplotype of the upstream region of the *Eb* gene but with different haplotypes of downstream regions of the *Ea* gene (Table 1), and the disease severity was compared among these female F_1 mice.

Typing of H-2 Haplotype. Peripheral blood was obtained from the periorbital sinus, followed by lysis of red blood cells with ammonium chloride. Aliquots of 5×10^5 to 10×10^5 cells were incubated with anti-A^d (K24–199) (21); anti-E (ISCR, which reacts with a common determinant of the E molecule) (a kind gift from Dr. N. Shinohara, Kitasato University, Kanagawa, Japan); anti-D^d (T19–191); and anti-D^b (H141–30) mAbs, followed by FITC-labeled anti-mouse polyclonal IgG antibodies (ICN). Incubations were run for 30 min at 4°C, and the stained cells were analyzed by using FACSTAR and CELLQUEST software (Becton Dickinson).

Microsatellite DNA Polymorphism in the *Tnfa* Promoter. *Tnfa* promoter was shown to have microsatellite polymorphism, and different tumor necrosis factor alleles have different lengths of microsatellites (22, 23). To determine the tumor necrosis factor alleles of each mouse strain, PCRs were performed with genomic DNAs, using 5′ primer (5′-GGACAGAGAAGAAATGGGTTTC-3′) and 3′ primer (5′-TCGAATCTGGGGCCAATCAGGAGGG-3′) (22), and differences in lengths of PCR products were determined by using electrophoresis of PCR products on 7% denaturing polyacrylamide gels, as described in ref. 24.

Measurement of Proteinuria. The onset of renal disease was monitored by biweekly testing for proteinuria, as described in ref. 25. Mice with a proteinuria of 111 mg/ml or more in repeated tests were regarded as being positive.

Measurements of Anti-DNA and Anti-Chromatin Antibodies. Serum levels of IgG autoantibodies to DNA and chromatin were determined by ELISA, using peroxidase-conjugated polyclonal anti-mouse IgG antibodies (ICN). The DNA- and chromatin-binding activities were expressed in units, referring to a standard curve obtained by serial dilutions of a standard serum pool from 7- to 9-month-old (NZB × NZW)F_1 mice, containing 1,000 units/ml (5). DNA was obtained from calf thymus (Sigma). Chromatin was prepared as described in ref. 26. Briefly, nucleosomes were isolated by solubilizing chromatin from purified chicken erythrocyte nuclei with micrococcal nuclease. The solubilized chromatin was fractionated into sucrose gradients that were analyzed for monomers by using electrophoresis, and the appropriate fractions were dialyzed and pooled.

Analysis of T Cell Activation and T Cell Receptor (TCR) V_β Repertoires. To examine the activation states of $CD4^+$ T cells, aliquots of 10^6 spleen cells were double-stained with FITC-conjugated anti-CD4 mAb and phycoerythrin-conjugated anti-CD69 mAb. To analyze TCR V_β repertoires, spleen cells were stained with biotin-labeled mAbs to each TCR V_β repertoire (Pharmingen), followed by incubation with avidin-phycoerythrin and FITC-conjugated anti-CD4 mAb. All incubations were run for 30 min at 4°C, and the frequency of $CD4^+$ T cells with each TCR V_β repertoire per total $CD4^+$ T cells was calculated by using FACSTAR and CELLQUEST software.

Preparation of Retroviral Construct with Chromatin-Specific TCR Genes and Transduction to Splenocytes. Chromatin-specific TCR V_α and V_β DNA fragments were synthesized, using PCR based on the published sequences of the nucleosome-specific T cell line derived from the lupus-prone (SWR × NZB)F_1 mouse (27, 28), as described in ref. 29. These fragments were cloned into a pMXW retroviral vector (30) and transfected into PLAT-E packaging cell lines (31) by using FuGENE6 transfection reagent (Roche Diagnostics). The viral supernatant of transfected cells were placed on fibronectin-coated 24-well plates, and total spleen cells from 2-month-old (NZB × NZW)F_1 mice prestimulated for 48 h with Con A (10 μg/ml) and interleukin 2 (50 ng/ml) were added to the wells (1×10^6 cells per well). Cells were cultured further for 36 h to allow infection to occur.

Purification and Functional Analysis of Dendritic Cells (DCs). Spleen cells were treated with collagenase type IV (Sigma) and DNase I, and $CD11c^+$ cells were positively collected by passing spleen cells twice through MACS CD11c microbeads and magnetic separation columns. The purity (85% in average) of DCs was determined by flow cytometry with anti-CD11c-biotin, followed by streptavidin-phycoerythrin.

To analyze the potential of chromatin presentation, $CD4^+$ T cells were purified by negative selection, using MACS microbeads with anti-CD19, -CD11c, and -CD8 mAbs 24 h postinfection, and 2×10^4 cells per well of T cells were cocultured with 1×10^5 cells per well of irradiated $CD11c^+$ DCs in 96-well flat-bottom plates with 1 μg/ml chromatin. After 24 h of culture, the cells were pulse-labeled with 1 μCi (1 Ci = 37 GBq) of [^{3}H]thymidine per well (NEN) for 15 h, and the [^{3}H]thymidine incorporation was determined.

Statistical Analysis. Statistical analysis was performed by using Student's t test and the χ^2 test. $P < 5\%$ was considered to have a statistical significance.

Results

Establishment of Intra-MHC Recombinant-Congenic New Zealand Mice. By selective backcrossing, we first introduced the H-2^{g2} haplotype derived from the B10.GD strain into NZB (H-2^d) and NZW (H-2^z) and established H-2-congenic NZB.GD (20) and NZW.GD strains. H-2^{g2} has an intragenic recombination between d and b haplotype in the E gene and the H-2 haplotype is $K^dAb^dAa^dEb^dEa^bTnfa^bD^b$ (Table 1) (32). Because the Ea^b gene is defective, H-2^{g2} mice do not express E molecules (20). To establish the strain that carries the H-2 haplotype of $K^dAb^dAa^dEb^dEa^dTnfa^bD^b$, we conducted a search for the mouse with a spontaneously occurring intragenic recombination between Ea and $Tnfa$ in the progeny of NZB and NZB.GD crosses. In ≈3,000 meiosis, there was a single mouse carrying this recombination, and the recombination-congenic NZB line, provisionally designated NZB.GDr (H-2^{g2r}), was generated. This haplotype is valid to evaluate the effect of E molecule expression on the same $Tnfa^bD^b$ background. Table 1 summarizes the haplotypes of the intra-MHC-congenic New Zealand mouse and the related strains.

E Molecule Expression Levels in (NZB × NZW)F_1 Mice with Different Intra-H-2 Haplotypes. Congenic and recombinant-congenic New Zealand mice were crossed to obtain (NZB × NZW)F_1 mice with four different combinations of the H-2 haplotype (Table 1). Fig. 1 shows flow cytometric analyses for expression profiles of A, E, and D molecules on peripheral blood lymphocytes. As expected, although levels of A^d expression were almost identical, levels of E molecules differed significantly among these F_1 mice, i.e., full expression levels in H-$2^{d/d}$ homozygous, approximately one-half of expression levels in H-$2^{d/g2}$ and H-$2^{g2r/g2}$ heterozygous, and no expression in H-$2^{g2/g2}$ homozygous F_1 mice. Profiles of the class I D molecule expression showed that lymphocytes from H-$2^{d/g2}$ F_1 mice were positive for both D^d and D^b, whereas those from H-$2^{g2r/g2}$ and H-$2^{g2/g2}$ F_1 mice were positive for D^b and negative for D^d. As also shown in Fig. 1, E molecules in wild-type H-$2^{d/z}$ heterozygous F_1 mice were fully expressed. Because these F_1 mice are heterozygous H-$2^{d/z}$, the level of A^d and D^d expression was approximately one-half of that seen in the H-$2^{d/d}$ homozygote.

Comparisons of Disease Features. Fig. 2A compares cumulative incidences of proteinuria in wild-type H-$2^{d/z}$ heterozygous (NZB × NZW)F_1 mice with intact E molecule expression and four kinds of H-2-congenic (NZB × NZW)F_1 (H-$2^{d/d}$, H-$2^{d/g2}$, H-$2^{g2r/g2}$, and H-$2^{g2/g2}$) carrying identical homozygous $A^{d/d}$ molecules but different levels of E molecule expression. Compared with findings in wild-type F_1 mice, the incidence was markedly reduced in homozygous $A^{d/d}$ F_1 mice with intact E molecule expression (H-$2^{d/d}$). In a striking contrast, homozygous $A^{d/d}$ F_1 mice deficient in E expression (H-$2^{g2/g2}$) showed an early onset and a high incidence of proteinuria comparable to those found in the wild-type F_1 mice. Findings in H-$2^{d/g2}$ and H-$2^{g2r/g2}$ with one-half of E expression levels were in between. Together with the finding that heterozygous H-$2^{g2r/g2}$ and homozygous H-$2^{g2/g2}$ F_1 mice share the same H-2 haplotype except for the Ea subregion (Table 1), it is strongly suggested that the development of lupus nephritis in $A^{d/d}$ F_1 mice is down-regulated by E molecules in a dose-dependent manner.

As shown in Fig. 2B, the decrease in survival rate was associated with an increase in the incidence of proteinuria in all groups of mice. Whereas all H-$2^{g2/g2}$ F_1 mice and 90% of wild-type F_1 mice died of disease by 12 months of age, 80% of H-$2^{d/d}$ F_1 mice and ≈50% of H-$2^{d/g2}$ and H-$2^{g2r/g2}$ F_1 mice remained alive. In Fig. 2 C and D, we compare serum levels of IgG autoantibodies to DNA and to chromatin, respectively, in 6-month-old homozygous $A^{d/d}$ F_1 mice with different levels of E expression. Whereas H-$2^{g2/g2}$ F_1 mice lacking E molecules showed high levels of both autoantibodies, comparable to those found in wild-type F_1 mice, the levels were greatly reduced in mice expressing E molecules.

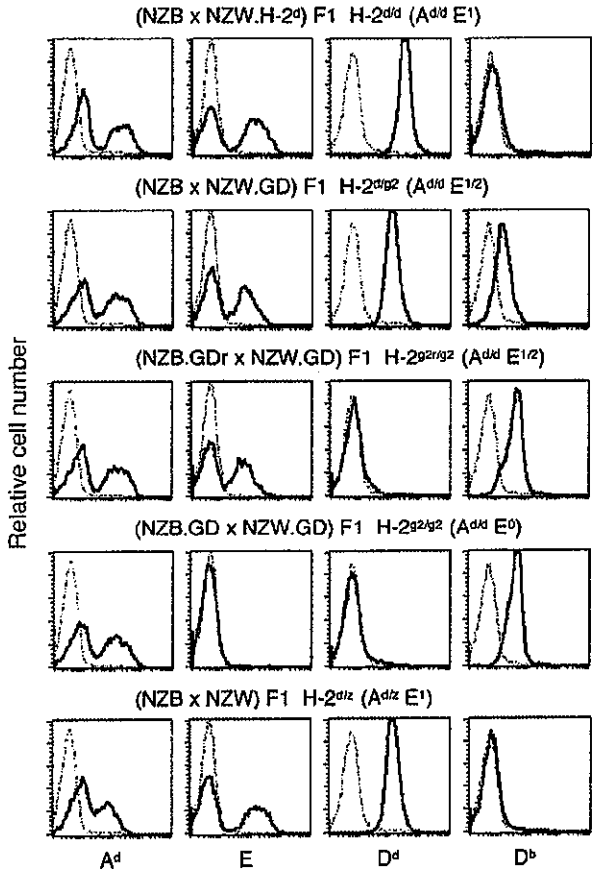

Fig. 1. Flow cytometry analysis for cell surface expression of A^d, E, D^d, and D^b molecules on peripheral lymphocytes in (NZB × NZW)F_1 mice with different H-2 haplotypes. The upper four groups of F_1 mice with homozygous $A^{d/d}$ showed the same expression level of A^d molecules, and the level in wild-type H-$2^{d/z}$ heterozygous F_1 mice was almost one-half of that seen in the former groups. When E molecule expression levels were examined with a mAb to a common determinant, H-$2^{d/g2}$ and H-$2^{g2r/g2}$ F_1 mice showed approximately one-half the level ($E^{1/2}$) of that seen in H-$2^{d/d}$ and wild-type H-$2^{d/z}$ F_1 mice (E^1). H-$2^{g2/g2}$ F_1 mice did not express E molecules (E^0). D^d expression levels in H-$2^{d/g2}$ and H-$2^{d/z}$ F_1 mice were approximately one-half of that seen in H-$2^{d/d}$ F_1 mice. D^b expression level in H-$2^{d/g2}$ F_1 mice was approximately one-half of that seen in H-$2^{g2r/g2}$ and H-$2^{g2/g2}$ F_1 mice.

Increase in Activated T Cells in E-Deficient Mice. Frequencies of $CD69^+$ activated $CD4^+$ T cells increase with age in (NZB × NZW)F_1 mice, as animals develop SLE (33). Fig. 3A compares frequencies of $CD69^+$ activated splenic $CD4^+$ T cells in total $CD4^+$ T cells among four groups of $A^{d/d}$ F_1 mice at 6 months of age. The frequency (mean ± SE) in E-negative H-$2^{g2/g2}$ F_1 mice (31.1 ± 8.6) was significantly higher than those found in three other groups of F_1 mice (11.0 ± 2.2 in H-$2^{d/d}$ F_1 mice, 14.2 ± 4.6 in H-$2^{d/g2}$ F_1 mice, and 17.2 ± 6.3 in H-$2^{g2r/g2}$ F_1 mice) ($P < 0.02$). Frequencies in H-$2^{d/g2}$ and H-$2^{g2r/g2}$ F_1 mice showed a tendency to be higher than those found in H-$2^{d/d}$ F_1 mice; however, there were no significant differences among the groups.

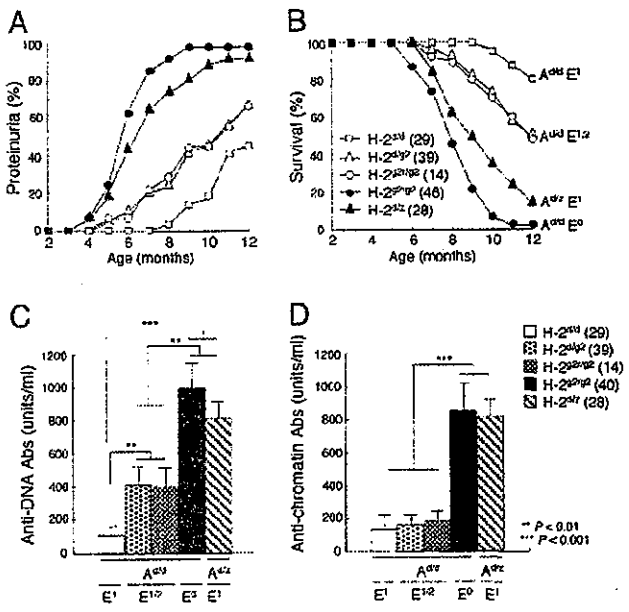

Fig. 2. Comparisons of the cumulative incidence of proteinuria (*A*), survival rate (*B*), and serum levels of IgG anti-DNA antibodies (*C*) and anti-chromatin antibodies (*D*) among F_1 mice with different H-2 haplotypes. The number of mice examined is shown in parentheses. H-$2^{g2/g2}$ F_1 showed a significantly higher incidence of proteinuria and a lower survival rate, as compared with three other $A^{d/d}$ F_1 strains ($P < 0.001$). Incidence of proteinuria and survival rate in H-$2^{d/d}$ F_1 mice were significantly reduced, as compared with H-$2^{d/g2}$ F_1 and H-$2^{g2r/g2}$ F_1 mice ($P < 0.01$). Compared with H-$2^{g2/g2}$ F_1 mice, wild-type H-$2^{d/z}$ F_1 mice showed a subtle but significantly lower incidence of proteinuria after 7 months of age ($P < 0.05$) and an improved survival rate after 9 months of age ($P < 0.05$). Serum levels of autoantibodies are compared at 6 months of age. Column and bar represent mean and SE, respectively. Asterisks indicate a significant difference.

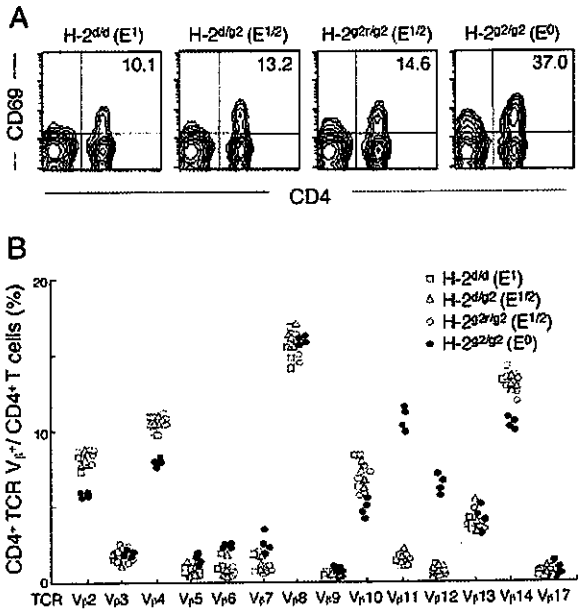

Fig. 3. Changes in splenic $CD4^+$ T cells among 6-month-old $A^{d/d}$ F_1 mice with different E molecule expression levels. (*A*) Representative flow cytometry profiles for the expression of activation marker CD69 on splenic $CD4^+$ T cells. Frequency of $CD69^+CD4^+$ T cells per total $CD4^+$ T cells is shown. (*B*) Comparisons of each TCR V_β repertoire frequency in splenic $CD4^+$ T cells. $V_\beta 11$ and $V_\beta 12$ repertoires were significantly higher in H-$2^{g2/g2}$ F_1 mice than those in other three F_1 mice ($P < 0.001$).

TCR V_β Repertoire Skewing in E-Deficient Mice. E molecule expression levels on thymic epithelial cells affect TCR V_β repertoire selection in the thymus (34–36). As shown in Fig. 3*B*, $V_\beta 11$ and $V_\beta 12$ repertoires in splenic $CD4^+$ T cells were negatively selected in E molecule-positive H-$2^{d/d}$, H-$2^{d/g2}$, and H-$2^{g2r/g2}$ F_1 mice, and there was no significant difference in these repertoire frequencies among the three groups. In contrast, significant proportions of $V_\beta 11$ (mean and SE, 10.8 ± 0.2%) and $V_\beta 12$ (6.0 ± 0.3%) repertoires were observed in E-negative H-$2^{g2/g2}$ F_1 mice.

Effects of E Molecule Expression on DC Function. Differences in haplotypes of class II molecules may affect autoimmune manifestations through the self-antigen presenting capacity of antigen-presenting cells. To determine whether the presence or absence of E molecules affects the potential for self-antigen presentation, we took advantage of a T cell proliferation assay against self-antigen. Splenic T cells from (NZB × NZW)F_1 mice were transfected *in vitro* with chromatin-specific TCR V_α and V_β, originally derived from a (SWR × NZB)F_1 mouse, which can recognize the immunodominant nucleosomal epitope (amino acids 71–94 in histone H4) in the context of $A^{d/d}$ (27, 28) and other A haplotype molecules (37). These T cells can reconstitute the specificity to the nucleosome (38). Such T cells and the T cells transfected with vector alone (mock) were cocultured with CD11c-positive splenic DCs obtained from (NZB × NZW)F_1 with different levels of E expression, in the presence of chromatin. As shown in Fig. 4, although DCs from $A^{d/d}$ F_1 mice with H-$2^{d/d}$, H-$2^{d/g2}$, and H-$2^{g2/g2}$ haplotypes induced significant levels of chromatin-specific T cell responses, there were no significant differences among the three groups of F_1 mice. Compared with findings in these $A^{d/d}$ F_1 mice, DCs from wild-type $A^{d/z}$ heterozygous (NZB × NZW)F_1 mice induced a significantly greater response of chromatin-specific T cells. Thus, it is suggested that, as compared with $A\alpha^d\beta^d$, $A^{d/z}$-unique $A\alpha^d\beta^z$ and/or $A\alpha^z\beta^d$ have an increased capacity of DCs to present chromatin and that the presence or absence of E molecules does not influence the potential of DCs for chromatin presentation.

Discussion

Our newly generated intra-MHC recombinant-congenic (NZB × NZW)F_1 mice make it feasible to examine the role of class II A and E molecules in the regulation of autoimmune disease, with disregard to the effect of other MHC genes such as *Tnfa* and class I D, which also have been implicated in autoimmune susceptibility (39, 40). The results clearly indicated that class II A and E serve as promoting and protective genetic elements, respectively.

H-$2^{d/z}$ heterozygosity has a strong impact on SLE in (NZB × NZW)F_1 mice, because the disease is largely reduced in H-$2^{d/d}$ and H-$2^{z/z}$ homozygous mice (2, 3, 5). This observation means that a combination of H-2-linked genes from both parents play a role in an epistatic manner. In this context, we earlier speculated that the polymorphic class II α and β chain genes from both parents may form F_1-unique mixed haplotype α/β heterodimers, such as $A\alpha^d\beta^z$ and $A\alpha^z\beta^d$, either of which may serve as a restriction element for self-reactive T cells (5). Consistent was the finding in the present studies that, compared with DCs from $A^{d/d}$ homozygous F_1 mice, DCs from wild-type $A^{d/z}$ (NZB × NZW)F_1 mice showed a greater likelihood of chromatin presentation to T cells. Because the antigen-presenting capacity was not influenced by the presence or absence of E molecules, class II A molecules can be attributed to this event. The importance of mixed haplotype α/β heterodimers also was supported by findings of Gotoh *et al.* (7), in

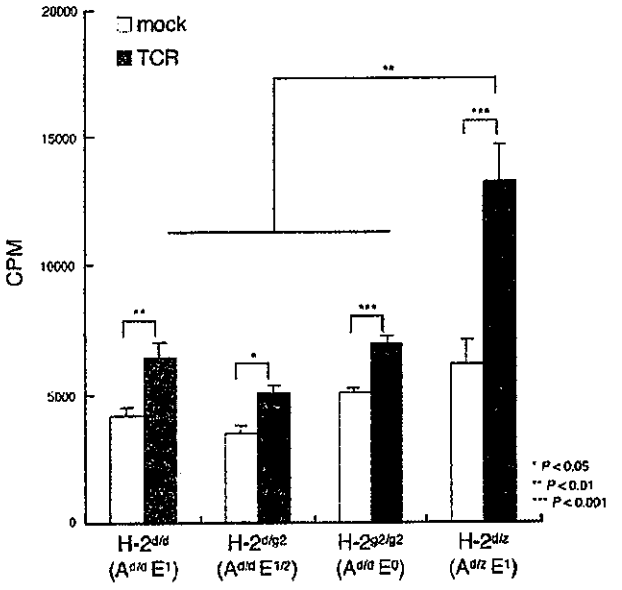

Fig. 4. The potential for chromatin presentation by CD11c-positive splenic cells from (NZB × NZW)F_1 mice with different H-2 haplotypes. Splenic T cells from (NZB × NZW)F_1 mice transfected with chromatin-specific TCR V_α and V_β or with vector alone (mock) were cocultured with CD11c-positive splenic DCs obtained from F_1 mice with different H-2 haplotypes, in the presence of chromatin, and T cell proliferative responses were compared. DCs from all these F_1 mice induced significant levels of chromatin-specific T cell responses; however, the potential of DCs for chromatin presentation was significantly higher in wild-type H-$2^{d/z}$ F_1 mice than that in other F_1 groups. Means and SE of three experiments are shown.

which the $A\alpha^d\beta^z$-restricted self-reactive T cell clone isolated from (NZB × NZW)F_1 mice had a potential to induce IgG anti-DNA antibodies *in vivo* (8). These F_1-unique mixed haplotype class II α/β heterodimers also may be involved in the aberrant selection of self-reactive T cells in the thymus. Based on studies by Braunstein and Germain (41), the assembly of $A\alpha$ and $A\beta$ chains of different haplotypes is under serious pairing restrictions. Thus, low expression levels of these heterodimers in the thymic epithelial cells may allow α/β heterodimer-restricted self-reactive T cells to escape from negative selection in the thymus.

In contrast to A molecules, the mixed-haplotype E molecules are not formed in most of the H-2 heterozygotes, because $E\alpha$ chains are usually nonpolymorphic (42). However, $E\alpha^z$ is unique among the $E\alpha$ chains of other haplotypes and has two amino acid substitutions in the α1 domain (43, 44). Thus, F_1 unique E molecules can be formed in H-$2^{d/z}$ F_1 mice. In this context, Nygard *et al.* (45) proposed the possible preferential formation of $E\alpha^d\beta^z$ mixed haplotype molecules and their involvement in the promotion of F_1 disease. However, evidence indicated that $E\alpha^d\beta^z$ molecules are protective rather than promoting (20).

The protective mechanism by E molecules remains elusive; however, several possibilities are suggested. First is the E-mediated clonal deletion model of self-reactive T cells in the thymus. It has been shown that T cells bearing TCR $V_\beta5$, $V_\beta11$, $V_\beta12$, and $V_\beta17a$ are eliminated in E-positive strains of mice (34–36), although the extent of negative selection is influenced by background genes (46–48). In this context, there are reports indicating that no clear-cut difference in the expression of TCR V_β repertoire was observed between E^+ and E^- transgenic NOD (16) as well as collagen-induced arthritis-susceptible B10.RQB3 mice (49), although the E transgene protected against the disease. Hence, the clonal deletion hypothesis for E-mediated protection of autoimmune disease has been dismissed in cases of these models. In the (NZB × NZW)F_1 genetic background, however, CD4 T cell repertoires bearing TCR $V_\beta11$ and $V_\beta12$ were significantly negatively selected in mice expressing E molecules. Thus, clonal deletion remains one possible mechanism at work in our mouse models.

Second is the determinant capture model. In *$E\alpha^d$*-transgenic BXSB mice, transgene-derived $E\alpha^d$ peptides bind to A^b molecules, possibly decreasing the use of A molecules for presentation of pathogenic self-peptides (18). Rudensky *et al.* (50) showed evidence for the binding of $E\alpha^d$ peptides to A^b molecules in a sequence analysis of peptides derived from the cell surface. This mechanism may be involved in the E-transgene-mediated protection of the collagen-induced arthritis model of $E\beta$-deficient B10.RQB3 mice (51, 52). However, such a mechanism may not be operative in our model, because the potential for chromatin presentation by $CD11C^+$ DCs was not affected by E molecules expressed in $A^{d/d}$ F_1 mice. This notion is in agreement with the finding by Nakano *et al.* (53) that antigen-presenting cells from both E^+ and E^- NOD mice can similarly stimulate diabetogenic T cells.

Third is the cytokine balance model. Hanson *et al.* (19) proposed that E molecule-mediated Th1/Th2 cytokine imbalance is one possible mechanism for the disease protection in $E\alpha^d$-transgenic NOD mice. Indeed, there is evidence that the differential MHC class II expression on antigen-presenting cells mediated by class II promoter polymorphism exerts a codominant effect on the Th1/Th2 cytokine balance (54, 55). In our preliminary studies, however, there was no clear difference in the potential of anti-CD3-stimulated T cells to produce IL-4 and IFN-γ between E^+ and E^- $A^{d/d}$ F_1 mice (data not shown).

An alternative is the signal transducer competition model, in which B cells may be the major cellular sites of E molecule-mediated autoimmune protection. Lang *et al.* (56) reported that antigen stimulation by means of the B cell antigen receptor on resting B cells induces association of MHC class II molecules with B cell antigen receptor-derived Ig-α/Ig-β heterodimers, which function as signal transducers on class II aggregation by the TCR. Because both A and E molecules physiologically associate with Ig-α/β heterodimers (56), when self-reactive B cells were stimulated by A-restricted T helper cells plus self-peptides, E molecules possibly associate competitively with Ig-α/β heterodimers. Hence, activation signals should be lower in E^+ than in E^- B cells. This idea well explains the observed dose dependency of E-mediated protection of SLE seen in the present studies.

Wild-type H-$2^{d/z}$ F_1 mice develop severe SLE, although they do express intact E molecules. This finding is in striking contrast to findings in H-$2^{d/d}$ F_1 mice that develop the disease only when lacking E molecules. Two mechanisms are thought to be involved. First, compared with H-$2^{d/d}$ F_1, the self-antigen-presenting capacity of DCs in H-$2^{d/z}$ F_1 is much higher, so that effects of E molecules may be insufficient for suppression. Alternatively, although not mutually exclusive, generation of H-$2^{d/z}$ F_1-unique self-reactive T cells restricted to haplotype-mismatched $A\alpha/\beta$ heterodimers in the thymus, as discussed above, may play a role in an E molecule-independent manner.

Taken collectively, our mouse models may provide means for further clarification of molecular mechanisms involved in the positive and negative regulation of autoimmune disease mediated by class II A and E molecules. Studies on the suppressive effect of E molecules are of particular importance, because one can apply this knowledge to future prophylactic and therapeutic approaches to autoimmune diseases.

We thank Prof. S. Matsushita (Saitama Medical School, Saitama, Japan) for helpful discussion and M. Ohara (Fukuoka, Japan) for language assistance. This work was supported in part by a Grant-in-Aid for

Scientific Research (B) for Scientific Research on Priority Areas and for Center of Excellence Research from the Ministry of Education, Science, Technology, Sports, and Culture of Japan and a grant from the Organization for Pharmaceutical Safety and Research (Japan).

1. Tsao, B. P. (2002) in *Dubois' Lupus Erythematosus*, eds. Wallace, D. J. & Hahn, B. H. (Lippincott Williams & Wilkins, Philadelphia), pp. 97–119.
2. Hirose, S., Nagasawa, R., Sekikawa, I., Hamaoki, M., Ishida, Y., Sato, H. & Shirai, T. (1983) *J. Exp. Med.* **158**, 228–233.
3. Hirose, S., Ueda, G., Noguchi, K., Okada, T., Sekigawa, I., Sato, H. & Shirai, T. (1986) *Eur. J. Immunol.* **16**, 1631–1633.
4. Kotzin, B. L. & Palmer, E. (1987) *J. Exp. Med.* **165**, 1237–1251.
5. Hirose, S., Kinoshita, K., Nozawa, S., Nishimura, H. & Shirai, T. (1990) *Int. Immunol.* **2**, 1091–1095.
6. Kono, D. H., Burlingame, R. W., Owens, D. G., *Kuramochi, A.*, Balderas, R. S., Balomenos, D. & Theofilopoulos, A. N. (1994) *Proc. Natl. Acad. Sci. USA* **91**, 10168–10172.
7. Gotoh, Y., Takashima, T., Noguchi, K., Nishimura, H., Tokushima, M., Shirai, T. & Kimoto, M. (1993) *J. Immunol.* **150**, 4777–4787.
8. Tokushima, M., Koarada, S., Hirose, S., Gotoh, Y., Nishimura, H., Shirai, T., Miyake, K. & Kimoto, M. (1994) *Immunology* **83**, 221–226.
9. Murphy, E. D. & Roths, J. B. (1979) *Arthritis Rheum.* **22**, 1188–1194.
10. Merino, R., Fossati, L., Lacour, M., Lemoine, R., Higaki, M. & Izui, S. (1992) *Eur. J. Immunol.* **22**, 295–299.
11. Merino, R., Iwamoto, M., Fossati, L., Muniesa, P., *Araki, K., Takahashi, S.*, Huarte, J., Yamamura, K. I., Vassalli, J. D. & Izui, S. (1993) *J. Exp. Med.* **178**, 1189–1197.
12. Hattori, M., Buse, J., Jackson, R., Glimcher, L., Dorf, M., Minami, M., Makino, S., Moriwaki, K., Kuzuya, H., Imura, H., *et al.* (1986) *Science* **231**, 733–735.
13. Acha-Orbea, H. & McDevitt, H. (1987) *Proc. Natl. Acad. Sci. USA* **84**, 2435–2439.
14. Nishimoto, H., Kikutani, H., Yamamura, K. & Kishimoto, T. (1989) *Nature* **328**, 432–434.
15. Lund, T., O'Reilly, L., Hutchings, P., Kanagawa, O., Simpson, E., Gravely, R., Chandler, P., Dyson, J., Picard, J., Edwards, A., *et al.* (1990) *Nature* **345**, 727–729.
16. Bohme, J., Schuhbaur, B., Kanagawa, O., Benoist, C. & Mathis, D. (1990) *Science* **249**, 293–295.
17. Labrecque, N., Madsen, L., Fugger, L., Benoist, C. & Mathis, D. (1999) *Immunity* **11**, 515–516.
18. Iwamoto, M., Ibnou-Zekri, N., Araki, K. & Izui, S. (1996) *Eur. J. Immunol.* **26**, 307–314.
19. Hanson, M. S., Cetkovic-Cvrlje, M., Ramiya, V. K., Atkinson, M. A., Maclaren, N. K., *Singh, B.*, Elliott, J. F., Serreze, D. V. & Leiter, E. H. (1996) *J. Immunol.* **157**, 1279–1287.
20. Hirose, S., Zhang, D., Nozawa, S., Nishimura, H. & Shirai, T. (1994) *Immunogenetics* **40**, 150–153.
21. Figueroa, F., Tewarson, S., Neufeld, E. & Klein, J. (1982) *Immunogenetics* **15**, 431–436.
22. Jongeneel, C. V., Acha-Orbea, H. & Blankenstein, T. (1990) *J. Exp. Med.* **171**, 2141–2146.
23. Jacob, C. O., Hwang, F., Lewis, G. D. & Stall, A. M. (1991) *Cytokine* **3**, 551–561.
24. Fujimura, T., Hirose, S., Jiang, Y., Kodera, S., Ohmuro, H., Zhang, D., Hamano, Y., *Ishida, H.*, Fukukawa, S. & Shirai, T. (1998) *Int. Immunol.* **10**, 1467–1472.
25. Knight, J. G. & Adams, D. D. (1976) *J. Exp. Med.* **147**, 1653–1660.
26. Bates, D. L., Butler, P. J., Pearson, E. C. & Thomas, J. O. (1981) *Eur. J. Biochem.* **119**, 469–476.
27. Mohan, C., Adams, S., Stanik, V. & Datta, S. K. (1993) *J. Exp. Med.* **177**, 1367–1381.
28. Kaliyaperumal, A., Mohan, C., Wu, W. & *Datta, S. K.* (1996) *J. Exp. Med.* **183**, 2459–2469.
29. Fujio, K., Misaki, Y., Setoguchi, K., Morita, S., Kawahata, K., Kato, I., Nosaka, T., Yamamoto, K. & Kitamura, T. (2000) *J. Immunol.* **165**, 528–532.
30. Zufferey, R., Donello, J. E., Trono, D. & Hope, T. J. (1999) *J. Virol.* **73**, 2886–2892.
31. Morita, S., Kojima, T. & Kitamura, T. (2000) *Gene Ther.* **7**, 1063–1066.
32. Lilly, F. & Klein, Y. (1973) *Transplantation* **16**, 530–532.
33. Ishikawa, S., Akakura, S., Abe, M., Terashima, K., Chijiiwa, K., Nishimura, H., Hirose, S. & Shirai, T. (1998) *J. Immunol.* **161**, 1267–1273.
34. Kappler, J. W., Roehm, N. & Marrack, P. (1987) *Cell* **49**, 273–280.
35. Bill, J., Appel, V. & Palmer, E. (1988) *Proc. Natl. Acad. Sci. USA* **85**, 9184–9188.
36. Bill, J., Kanagawa, O., Woodland, D. L. & Palmer, E. (1989) *J. Exp. Med.* **169**, 1405–1419.
37. Shi, Y., Kaliyaperumal, A., Lu, L., Southwood, S., Sette, A., Michaels, M. A. & Datta, S. K. (1998) *J. Exp. Med.* **187**, 367–378.
38. Fujio, K., Okamoto, A., Tahara, H., Abe, M., Jiang, Y., Kitamura, T., Hirose, S. & Yamamoto, K. (2004) *J. Immunol.* **173**, 2118–2125.
39. Jacob, C. O. & McDevitt, H. O. (1988) *Nature* **331**, 356–358.
40. La Cava, A., Balasa, B., Good, A., *van Gunst, K.*, Jung, N. & Sarvetnick, N. (2001) *J. Immunol.* **167**, 1066–1071.
41. Braunstein, N. S. & Germain, R. N. (1987) *Pro. Natl. Acad. Sci. USA* **84**, 2921–2925.
42. Mathis, D. J., Benoist, C. O., Williams, V. E., II, Kanter, M. R. & McDevitt, H. O. (1983) *Cell* **32**, 745–754.
43. Sciffenbauer, J., McCarthy, D. M., Nygard, N. R., Woulfe, S. L., Didier, D. K. & Schwartz, B. D. (1989) *J. Exp. Med.* **170**, 971–984.
44. Ogawa, S., Nishimura, H., Awaji, M., Nozawa, S., Hirose, S. & Shirai, T. (1990) *Immunogenetics* **32**, 63–67.
45. Nygard, N. R., McCarthy, D. M., Schiffenbauer, J. & Schwartz, B. D. (1993) *Immunol. Today* **14**, 53–56.
46. Kappler, J. W., Staerz, U., White, J. & Marrack, P. (1987) *Nature* **332**, 35–40.
47. MacDonald, H. R., Schneider, R., Lees, R. K., Howe, R. C., Acha-Orbea, H., Festenstein, H., Zinkernargel, R. M. & Hengartner, H. (1988) *Nature* **332**, 40–45.
48. Pullen, A. M., Marrack, P. & Kappler, J. W. (1988) *Nature* **335**, 796–801.
49. Gonzalez-Gay, M. A., Nabozny, G. H., Bull, M. J., Zanelli, E., Douhan, J., III, Griffiths, M. M., Glimcher, L. H., Luthra, H. S. & David, C. S. (1994) *J. Exp. Med.* **180**, 1559–1564.
50. Rudensky, A. Y., Preston-Hurlburt, P., Hong, S. C., Barlow, A. & Janeway, C. A., Jr. (1991) *Nature* **353**, 622–627.
51. Gonzalez-Gay, M. A., Zanelli, E., Kreo, C. J., Nabozny, G. H., Hanson, J., Griffiths, M. M., Luthra, H. S. & David, C. S. (1995) *Immunogenetics* **42**, 35–40.
52. Gonzalez-Gay, M. A., Zanelli, E., Khare, S. D., Kreo, C. J., Griffiths, M. M., Luthra, H. S. & David, C. S. (1996) *Immunogenetics* **44**, 377–384.
53. Nakano, N., Kikutani, H., Nishimoto, H. & Kishimoto, H. (1991) *J. Exp. Med.* **173**, 1091–1097.
54. Guardiola, J., Maffei, A., Lauster, R., Mitchison, N. A., Accolla, R. S. & Sartoris, S. (1996) *Tissue Antigens* **48**, 615–625.
55. Baumgard, M., Moos, V., Schuhbauer, D. & Müller, B. (1998) *Proc. Natl. Acad. Sci. USA* **95**, 6936–6940.
56. Lang, P., Stolpa, J.C., Freiberg, B. A., Crawford, F., Kappler, J., Kupfer, A. & Cambier, J. C. (2001) *Science* **291**, 1537–1540.

Available online at www.sciencedirect.com
SCIENCE DIRECT®
Analytical Biochemistry 337 (2005) 316–324
ANALYTICAL BIOCHEMISTRY
www.elsevier.com/locate/yabio

Isolation and mass spectrometry characterization of molecular species of lactosylceramides using liquid chromatography-electrospray ion trap mass spectrometry

Naoko Kaga[a], Saiko Kazuno[a], Hikari Taka[a], Kazuhisa Iwabuchi[b,c], Kimie Murayama[a,*]

[a] *Division of Proteomics and Biomolecular Science, BioMedical Research Center, Juntendo University Graduate School of Medicine, Tokyo 113-8421, Japan*
[b] *Institute for Environmental and Gender-Specific Medicine, Juntendo University Graduate School of Medicine, Tokyo 113-8421, Japan*
[c] *Laboratory of Biochemistry, Juntendo University School of Healthcare and Nursing, Chiba, Japan*

Received 27 September 2004
Available online 2 December 2004

Abstract

Reverse-phase liquid chromatography/electrospray ion trap mass spectrometry (LC-ESI-MS^n) was established for identification of the molecular species of lactosylceramides. Lactosylceramides derived from porcine blood cells were separated on a CapcellPak C_8 column using a mixture of methanol and 1 mM ammonium formate from the C_{16} to C_{26} fatty acyl chains based on the length of total carbon chains and the nature of sphingoid bases (w'') and fatty acyl chains ($Y'_0 - w''$) was identified by MS^3 as their $[M + H]^+$ ions. The same number of fatty acyl moieties appeared in the order of unsaturated, (2-)hydroxylated, and saturated components. The molecular species of lactosylceramides derived from porcine blood cells totaled more than 33 and included mainly $C_{24:0}$-$d_{18:1}$, $Ch_{24:0}$-$d_{18:1}$, $Ch_{24:1}$-$d_{18:1}$, $C_{24:1}$-$d_{18:1}$, and $C_{22:0}$-$d_{18:1}$ in addition to 28 minor species from $C_{16:0}$ to $C_{26:0}$ fatty acyl moieties. The molecular species of lactosylceramides in the membrane microdomain fraction of HL-60 cells (70% were differentiated into macrophage-lineage cells) were identified as $C_{24:0}$-$d_{18:1}$, $C_{24:1}$-$d_{18:1}$, $C_{22:0}$-$d_{18:1}$, $C_{16:0}$-$d_{18:1}$, and more than 21 other minor species. Our results suggest that reverse-phase LC-ESI-MS^n is a useful and simple method for identification of lactosylceramide molecular species.

Keywords: Lactosylceramide; Molecular species; Fatty acyl chain moiety; Long-chain base moiety; LC-ESI-MS^n

Studies on molecular membrane biology have focused on the dynamics of cellular proteins and the lipid microenvironment at the cell surface [1]. It is known that glycosphingolipids play important roles in cell–cell interaction, recognition, transmembrane signaling, and cellular growth and differentiation in animal cells [2]. These compounds self-aggregate easily based on their nature and cluster with sphingomyelin with or without cholesterol and various signal transducer molecules to form various types of microdomains called "lipid-raft" at plasma membrane [3–6]. Although the lipid composition of the rafts in different cells is not clear, lactosylceramides are known to localize with "sphingolipid-sterol rafts" and trigger raft-related signal transduction processes. In neutrophils, lactosylceramide-enriched microdomains on the cell surface coupled with tyrosine protein kinase LYN (Lyn)[1] induce the activation of Lyn via lactosylceramides and lead to superoxide generation [3].

To understand the biological activity and physical behavior of lactosylceramides, it is important to deter-

* Corresponding author. Fax: +81 3 3818 6330.
E-mail address: murayama@med.juntendo.ac.jp (K. Murayama).

[1] *Abbreviations used:* Lyn, tyrosine protein kinase LYN; FAB, fast atom bombardment; CAD, collisional-activated dissociation; CID, collision-induced dissociation; ESI, electrospray ionization; APCI, atmospheric pressure chemical ionization; DFP, diisopropylphosphorofluoridate; SIM, single ion monitoring; 3D, three-dimensional.

0003-2697/$ - see front matter © 2004 Elsevier Inc. All rights reserved.
doi:10.1016/j.ab.2004.11.003

mine their structural heterogeneity. Lactosylceramides contain lactose and a ceramide moiety. Various classes of the sphingoid base have been identified, such as the dihydro type (sphinganine), the additional hydroxyl group type (phytosphingosine), and the 2-amino-4-ene-1,3-diol type with 14–22 carbon chains (sphingenine). The commonest type in animal tissues is C_{18} sphingenine ($-d_{18:1}$). In addition, significant variation can also occur in fatty acyl moiety with regard to chain length, unsaturation, and hydroxylation. Lactosylceramides containing saturated fatty acyl chains display relatively high thermotropic and pressure-induced transition, but the introduction of a single *cis* double bond into the fatty acyl chains markedly reduce these properties, especially when the double bonds are located near the middle of the fatty acyl chain [6].

Mass spectrometry (MS) is a powerful tool for lipid structure analysis. Several methods incorporating tandem MS for identification of intact ceramides and neutral sphingolipids such as glucosyl- and lactosylceramides have been published. In early 1990s, Costello and Vath [7] used fast atom bombardment tandem mass spectrometry (FAB-MS/MS) and reported valuable data about the structure of glycosphingolipids, such as the molecular weight of fatty acyl chain and sphingoid base, by analyzing the MS/MS spectra of $[M+H]^+$ and $[M-H]^-$ ions. Ann and Adams [8,9] and Duarte et al. [10] also reported that, in the presence of alkaline metal, $[M+\text{metal}]^+$ ions were formed with ceramides and glucosylceramides and these showed a much higher sensitivity than the $[M+H]^+$ ions. In addition, they provided more informative MS/MS spectra for the location of double bonds at high-energy CAD, by using charge remote cleavage. At present, electrospray ionization tandem mass spectrometry (ESI-MS/MS) and atmospheric pressure chemical ionization tandem mass spectrometry (APCI-MS/MS) are used for determination of the structure of intact ceramides and lactosylceramides with low-energy CID [11–13] or high-energy CID [14]. Lee et al. [15] and Pettus et al. [16] reported analysis of the molecular species of ceramides by reverse-phase LC-ESI/MS/MS and normal-phase LC-APCI/MS/MS, respectively.

We report here the design of a simple and useful method for separation and MS^n characterization of molecular species of lactosylceramides using reverse-phase HPLC-ESI ion trap mass spectrometry.

Materials and methods

Materials

Lactosylceramide derived from porcine blood cells was purchased from Matreya (Pleasant Gap, PA). The synthetic lactosylceramide for $C_{24:1}$-$d_{18:1}$ was provided by Professor Sandro Sonnino (Center of Excellence on Neurodegenerative Diseases, Department of Medical Chemistry, Biochemistry and Biotechnology, University of Milan, Italy). All reagents used in this study were of the highest grade, especially those used for HPLC, spectrometry, and amino acid analysis. Chloroform, acetone, sodium chloride, methanol, ethylenediaminetetraacetic acid (EDTA), Triton X-100, Tris–HCl, vitamin D_3, and diisopropylphosphorofluoridate (DFP) were purchased from Wako Pure Chemical Industries (Osaka, Japan). Lithium chloride anhydrous and ethylene glycol bis (β-aminoethyl ether)-*N,N,N′,N′*-tetraacetic acid (EGTA) were obtained from Nacalai Tesque (Kyoto, Japan). Ammonium acetate, ammonium formate, and primulin were from Sigma–Aldrich (St. Louis, MO). Complete is a product of Roche (Switzerland). Ultrapure water was prepared using the Millipore Milli-Q purification system (Bedford, MA).

Mass spectrometric analysis

All analyses were performed in positive mode using a LCQ DECA XP ion trap mass spectrometer (Thermo Electron, San Jose, CA) with a conventional electrospray ionization source.

Infusion-ESI-MS^n analysis

Lactosylceramide at a concentration of 5–10 ng/μl was dissolved in methanol with or without alkaline and ammonium salts (1 mM LiCl, 1 mM NaCl, and 10 mM ammonium acetate). Sample solution was directly infused at a rate of 3–5 μl/min into the ESI source without separation of the molecular species of lactosylceramides. The temperature of the ion transfer tube was set at 150–400 °C. The spray voltage was set at 5 kV and the nitrogen sheath gas pressure used was 10 U. In MS^n ($n = 2$–4) analysis, the collision energy was fixed at 100%.

HPLC-ESI-MS^n analysis. Reverse-phase HPLC was carried out with the Magic2002 system (Michrom BioResources, Auburn, CA). The column was Capcellpak C_8 UG120, 1.0 mm ID × 150 mm (Shiseido Fine Chemicals, Tokyo). The mobile phases were as follows: solvent A was 1 mM ammonium formate in methanol:water (76:24 v/v) and solvent B was 1 mM ammonium formate in methanol:water (96:4 v/v). The elution program was isocratic elution with 80% B for 5 min, increase to 95% B, and then hold for 30 min. The flow rate was 50 μl/min. The HPLC was joined to the mass spectrometer, LCQ DECA XP. The MS conditions were as follows: ion transfer tube temperature 250 °C, spray voltage 5 kV, sheath gas pressure 20 U. MS^n ($n = 4$) analysis was performed on data-dependent experiments (DDE) with collision energy 80%.

Identification of molecular species of lactosylceramides in the membrane microdomain fraction of HL-60 cells

Fractionation of the membrane microdomain fraction of HL-60 cells. Cells of the myeloid leukemia cell line HL-60 were maintained in RPMI 1640 medium supplemented with 10% fetal bovine serum. HL-60 cells (2×10^8 cells) were treated with active form vitamin D_3 (final concentration, 100 nM) for 5 days. Flow cytometric analysis using anti-CD11b antibody was performed as described previously [3]. Iwabuchi and Nagaoka [3] indicated that about 70% of the cells were differentiated into macrophage-lineage cells. Cells were resuspended in relaxation buffer (10 mM 1,4 piperazinedichanesulfonic acid, 100 mM KCl, 3 mM NaCl, 3.5 mM $MgCl_2$, and 1 mM ATP, pH 7.4) containing a mixture of protease inhibitors (1 mM phenylmethylsulfonyl fluoride, 0.4 μM aprotinin, 10 μM E-64, 20 μM leupeptin, 10 μM bestatin, 5 μM *N*-acetyl-Leu-Leu-Met-al, and 2 μM pepstatin) and disrupted by nitrogen cavitation (N_2 for 20 min at 350 psi). Disrupted cells were dropped gradually into EGTA solution (final concentration, 1.25 mM). All manipulations were carried out at 4 °C. The plasma membrane was fractionated after sequential centrifugation; 500*g* at 4 °C for 10 min, 8500*g* for 20 min, and 200,000*g* for 1 h. This fraction was suspended in TNE-T buffer [1% Triton X-100, 10 mM Tris–HCl (pH 7.5), 150 mM Nacl, 1 mM DFP] containing 1/20 Complete.

Extraction of crude lactosylceramides. The crude lipids in the membrane microdomain fraction were extracted with a chloroform:methanol mixture (2:1 v/v). A fifth of them (20 μl/100 μl crude lipids) were separated on a 10 × 10-cm high-performance thin-layer chromatography (HPTLC) plate (Merck, Rahway, NJ) with chloroform/methanol/water 65:25:4 (v/v/v). After development, lactosylceramides were visualized using primulin reagent (0.03% in 80% acetone) under ultraviolet light. Lactosylceramide-containing bands were scratched out from the plate and extracted with chloroform/methanol (2:1 v/v). After drying, lactosylceramides were dissolved in 20 μl of methanol and 4 μl of the solution was loaded on the column for LC-ESI-MS^n analysis. Finally, lactosylceramides from HL-60 (8×10^6 cells) were analyzed.

Results and discussion

Effects of salts and temperature on ionization of synthetic lactosylceramide at $C_{24:1}$-$d_{18:1}$

To compare the effects of salts and ion transfer tube temperature on ionization of lactosylceramide by infusion analysis, synthetic lactosylceramide at $C_{24:1}$-$d_{18:1}$ was dissolved in methanol with/without 1 mM LiCl, NaCl, or 10 mM ammonium acetate at 5 ng/μl and analyzed with the ion trap mass spectrometer. In salt-free condition, lactosylceramide at $C_{24:1}$-$d_{18:1}$ did not produce the $[M + H]^+$ ion at 400 °C, but the $[M + Na]^+$ ion, which was produced from concomitant sodium in the sample or reagents, was stable.

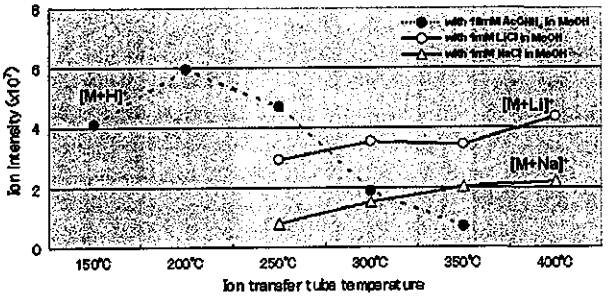

Fig. 1. Effects of salts and temperature on ionization of lactosylceramide by infusion analysis. Synthetic lactosylceramide of $C_{24:1}$-$d_{18:1}$ was dissolved in methanol containing each salt at 5 ng/μl concentration. The flow rate was 3 μl/min.

The addition of 1 mM NaCl to lactosylceramide markedly increased the amount of $[M + Na]^+$ ion at 400 °C (Fig. 1). On the other hand, the amount of $[M + Li]^+$ ion was twice as much as that of $[M + Na]^+$ ion at the same temperature. However, the addition of 10 mM ammonium acetate tended to produce the $[M + H]^+$ ion at 200 °C. The higher temperature (400 °C) for the $[M + H]^+$ ion was associated with the generation of dehydrated ion and resulted in a complex spectrum.

On the other hand, the $[M + Na]^+$ ion of lactosylceramide could not be produced at 200 °C. The optimal temperature of the ion transfer tube was 400 °C for the $[M + metal]^+$ ion and 200 °C for the $[M + H]^+$ ion.

MS^n analysis of $[M + Li]^+$ and $[M + H]^+$ ion to characterize fatty acyl chain and long-chain base moiety

We performed MS^n analysis for $[M + Li]^+$ and $[M + H]^+$ ion of synthetic lactosylceramide ($C_{24:1}$-$d_{18:1}$) at optimal temperature (Fig. 2). In MS^n analysis for $[M + Li]^+$ ion, following the loss of one or two hexose(s) $[Y_1, Y_0]$ and water [represented as ′, ″], a HCHO was eliminated to form $[a_2]$ ion[11] on the MS^2/MS^3 spectra (Fig. 2A). $[Y_0]$ and $[a_2]$ ions were extremely stable at 400 °C and no further cleavage occurred on the MS^4 spectrum. We could not obtain information on the fatty acyl chain and long-chain base, even though the dissociation energy increased up to 100%. However, lactosylceramides containing 2-hydroxy fatty acyl chain underwent marked cleavage of the N–CO bond on the MS^3 spectrum and characterized the fatty acyl chain (data not shown).

On the other hand, in MS^n analysis of $[M + H]^+$ ion, the loss of two hexoses and water $[Y_0']$ on the MS^2 spec-